

# Observing nulling of primordial correlations via the 21 cm signal

Shyam Balaji,<sup>1,\*</sup> H. V. Ragavendra,<sup>2,†</sup> Shiv K. Sethi,<sup>3,4,‡</sup> Joseph Silk,<sup>5,§</sup> and L. Sriramkumar<sup>4,¶</sup>

<sup>1</sup>*Laboratoire de Physique Théorique et Hautes Energies (LPTHE),*

*UMR 7589 CNRS & Sorbonne Université, 4 Place Jussieu, F-75252, Paris, France*

<sup>2</sup>*Department of Physical Sciences, Indian Institute of Science Education and Research Kolkata, Mohanpur, Nadia 741246, India*

<sup>3</sup>*Raman Research Institute, C. V. Raman Avenue, Sadashivanagar, Bengaluru 560080, India*

<sup>4</sup>*Centre for Strings, Gravitation and Cosmology, Department of Physics,*

*Indian Institute of Technology Madras, Chennai 600036, India*

<sup>5</sup>*Institut d'Astrophysique de Paris, UMR 7095 CNRS & Sorbonne Université, 98 bis boulevard Arago, F-75014 Paris, France*

The 21 cm line emitted by neutral hydrogen (HI) during the Dark Ages carries imprints of pristine primordial correlations. In models of inflation driven by a single, canonical scalar field, we show that a phase of ultra-slow-roll can lead to a *null* in *all* the primordial correlations at a specific wavenumber  $k_{\text{dip}}$ . We consider scenarios wherein the null in the correlations occurs over wave numbers  $1 \lesssim k_{\text{dip}} \lesssim 10 \text{ Mpc}^{-1}$ , and examine the prospects of detecting such a damping in the HI signal due to the nulls at the level of power and bi-spectra in future observational missions.

*Primordial correlations and 21 cm observations:* Cosmic inflation remains the most attractive paradigm for the generation of primordial perturbations. On large scales, e.g. over  $10^{-5} \lesssim k \lesssim 1 \text{ Mpc}^{-1}$ , the primordial scalar power spectrum as generated in some of the popular models of slow roll (SR) inflation is remarkably consistent with the cosmic microwave background (CMB) anisotropies and large-scale structure (for a comprehensive list of inflationary models consistent with the Planck data, see Refs. [1, 2]). However, on smaller scales, e.g.  $k \gtrsim 1 \text{ Mpc}^{-1}$ , the constraints on the primordial scalar power spectrum are considerably weaker. Since the discovery of gravitational waves from merging binary black holes, the weaker constraints over small scales have been exploited to examine inflationary models which enhance power on these scales. This leads to significant production of primordial black holes and generation of secondary gravitational waves of observable strengths [3–16].

Often, in single field models of inflation involving the canonical scalar field, a phase of ultra-slow-roll (USR) is invoked to enhance the scalar power on small scales. The first SR parameter  $\epsilon_1$  exponentially decreases during such a phase, resulting in large values for the second and higher order SR parameters [4–6, 17, 18]. Such a departure from SR inflation leads to a peak in the inflationary scalar power spectrum and, generically, one finds that the power spectrum rises as  $k^4$  as it approaches the peak [19–21]. Interestingly, just before the power spectrum rises towards the peak, a sharp drop in power occurs [22] and, if the period of USR inflation is sufficiently long, the scalar power spectrum actually vanishes at a particular wavenumber, which we denote as  $k_{\text{dip}}$  [23]. This occurs because of the fact that the mode function describing the curvature perturbation corresponding to the wavenumber  $k_{\text{dip}}$  goes to zero at late times towards the end of inflation. It can immediately be shown that all of the higher correlations involving the curvature perturbation will also necessarily vanish at  $k_{\text{dip}}$ . In cases wherein the duration of USR is not sufficiently long, although a null does not arise, a sharp dip in the scalar power spectrum as well as in the higher order correlation functions is still encountered.

Over the scales  $1 \lesssim k \lesssim 10 \text{ Mpc}^{-1}$ , the 21 cm signal of neutral hydrogen (HI) from the Dark Ages carries the signatures of the primordial spectrum (see, e.g., Refs. [24, 25]). In contrast to the angular spectra of the CMB, which are a convolution of the primordial spectra and the transfer function of the photons, the features in the primordial power and bi-spectra leave direct and distinct imprints in the HI signal. Therefore, an inflationary feature such as a null or a sharp dip in the primordial correlations may potentially be observed in HI, if the features occur over the corresponding scales [26]. In this Letter, we consider specific scenarios involving a phase of USR inflation and investigate the effects of a dip on the HI signal at the level of both power and bi-spectra. If a drop in the scalar power spectrum is to occur over  $1 \lesssim k \lesssim 10 \text{ Mpc}^{-1}$ , we find that the CMB at smaller wavenumbers and the spectral distortions at higher wavenumbers limit the rise in power on small scales, and hence the extent of the dip. We calculate the corresponding observable signatures on the power and bi-spectra of the HI signal and discuss the prospects of observing them in future missions, such as a lunar array [27–29]. We also point out challenges that can arise due to Poisson fluctuations (PF) [30, 31].

*Nulls in inflationary correlations:* We now demonstrate that nulls in the inflationary correlations (i.e. in the scalar power spectrum as well as in higher order correlations) are expected to arise in scenarios involving a phase of USR inflation. Consider a situation wherein a regime of USR inflation is sandwiched between two epochs of SR inflation. Let  $\eta$  denote the conformal time coordinate, and let the two transitions between the three stages occur at the times  $\eta_1$  and  $\eta_2$ . Also, let the first SR parameter  $\epsilon_1$  prior to the first transition be a constant, say  $\epsilon_{1i} \lesssim 10^{-2}$ , while, during the period of USR, it is given by  $\epsilon_1 = \epsilon_{1i} (\eta/\eta_1)^6$ . Since  $\epsilon_1 \ll 1$  throughout the domains of interest, the Hubble parameter can be considered to be a constant, say,  $H_1$ , and hence the scale factor can be assumed to be of the de Sitter form.

Let us focus on the evolution of modes that leave the Hubble radius during the initial SR regime. In the first domain  $\eta < \eta_1$ , on super-Hubble scales, the mode function characterizing the curvature perturbation in Fourier space, say,  $f_k^I$ , can be expressed as

$$f_k^I(\eta) = C_k + \frac{D_k}{2} \eta^2. \quad (1)$$

The constants  $C_k$  and  $D_k$  can be determined by matching the super-Hubble solutions with the complete solution in the SR regime, and they are found to be  $C_k = i H_1 / (\sqrt{4k^3 \epsilon_{11}} M_{\text{pl}})$  and  $D_k = C_k k^2$ . During the USR phase, the modes function, say,  $f_k^{\text{II}}$ , for modes that are already on super-Hubble scales, can be expressed as

$$f_k^{\text{II}}(\eta) = A_k + B_k \left( \frac{1}{\eta^3} - \frac{1}{\eta_1^3} \right). \quad (2)$$

The quantities  $A_k$  and  $B_k$  can be determined by matching the mode functions and their time derivatives at the transition at  $\eta_1$  to obtain that  $A_k = C_k [1 + (k^2 \eta_1^2 / 2)]$  and  $B_k = -D_k \eta_1^5 / 3$ .

When the phase of USR ends, because the wavenumber of interest is on super-Hubble scales, its amplitude will evidently freeze at its value at the conformal time  $\eta_2$ . We should clarify that such a behavior can also be expected if, for  $\eta > \eta_2$ , the parameter  $\epsilon_1$  begins to grow leading to the termination of inflation. Hence, the power spectrum is determined by the value of  $f_k^{\text{II}}$  at  $\eta_2$ . Upon setting  $f_k^{\text{II}}(\eta_2)$  to be zero, we can immediately determine the wavenumber  $k_{\text{dip}}$  at which the amplitude of the curvature perturbation vanishes. It is given by

$$k_{\text{dip}} = -\frac{1}{\eta_1} \left\{ \frac{1}{3} \left[ \left( \frac{\eta_1}{\eta_2} \right)^3 - 1 \right] - \frac{1}{2} \right\}^{-1/2} \simeq \sqrt{3} k_1 e^{-3\Delta N/2}, \quad (3)$$

where the final expression has been arrived at by assuming that the epoch of USR is adequately long so that  $\eta_1/\eta_2 \gg 1$ , and we have set  $k_1 = -1/\eta_1$  (i.e. the wavenumber that leaves the Hubble radius at the onset of USR), while  $\Delta N$  denotes the duration of USR in e-folds. The power spectra and all the higher order correlations involve the mode function  $f_k$  evaluated towards the end of inflation. *Since the mode function  $f_k$  corresponding to the wavenumber  $k_{\text{dip}}$  vanishes at late times, any correlation function involving this mode necessarily vanishes as well.* However, if the duration of USR is not long enough (in fact, when  $e^{\Delta N} \lesssim 5/2$ ), then the mode function, rather than vanishing, settles down to a very small value at late times. In such cases, a sharp dip is produced rather than a null in the correlation functions, and the relation (3) predicts the location of the dip. Moreover, when the dominant term in the mode function  $f_k$  vanishes, the sub-dominant terms can lead to a small non-zero value at  $k_{\text{dip}}$ , resulting in a dip as opposed to a null.

*Inflationary models, power and bi-spectra:* To illustrate the nulls or dips that are expected in the correlation functions, we shall consider two models of inflation driven

by a single, canonical scalar field that permit a brief period of USR. These models should be treated as illustrative examples of inflationary scenarios generally considered to enhance power on small scales. We shall also briefly discuss a reconstructed scenario which easily allows us to achieve the desired background evolution and a power spectrum that is consistent with the constraints from the CMB on large scales.

The first model we shall consider is a model due to Starobinsky that is described by a linear potential with a sudden change in its slope [32–35]. It is one of the simplest models that leads to a regime of USR and a step-like feature in the scalar power spectrum. The potential describing the Starobinsky model (ST) is given by [32–35]

$$V(\phi) = \begin{cases} V_0 + A_+ (\phi - \phi_0) & \text{for } \phi > \phi_0, \\ V_0 + A_- (\phi - \phi_0) & \text{for } \phi < \phi_0, \end{cases} \quad (4)$$

where  $V_0$  sets the overall energy scale. Evidently,  $A_+$  and  $A_-$  determine the slopes of the potential on either side of  $\phi_0$ , and the slope is discontinuous at this point. Though there are issues in achieving a natural end to inflation, we consider the model because of its analytical tractability that helps in illustrating arguments related to features induced by USR (in this regard, see the supplementary material). In the model, the epoch of USR occurs when the field crosses  $\phi_0$  and the duration of this epoch is determined by the ratio of the slopes of the potential, i.e.  $A_-/A_+$ . It can be shown that, in the model,  $k_{\text{dip}} \simeq \sqrt{3} (A_-/A_+) k_0$ , where  $k_0$  is the wavenumber that leaves the Hubble radius when the field crosses  $\phi_0$  [32, 34, 36]. The parameters  $V_0$  and  $A_+$  are constrained by COBE normalization on the CMB scales (for values of the parameters, see the supplementary material, which includes Refs. [37, 38]). The constraints from spectral distortions over the wavenumbers  $1 < k < 10^4 \text{ Mpc}^{-1}$  limit the extent of enhancement in the power spectrum at small scales [39], and hence the duration of USR. We choose the parameters  $A_-$  and  $\phi_0$  so that the rise in power on smaller scales is consistent with the FIRAS constraints on  $\mu$  distortions [12]. Also, these parameters are chosen such that the dip in the power spectrum occurs at wavenumbers  $k \gtrsim 5 \text{ Mpc}^{-1}$  to evade bounds on the matter power spectrum from the Lyman- $\alpha$  data (see e.g., Refs. [30, 40]). For the parameters we work with, we find that  $k_{\text{dip}} = 7.6 \text{ Mpc}^{-1}$ . We should clarify that, the duration of USR in ST is determined by the ratio of  $A_-/A_+$ , which, in turn, determines the height of scalar power at its maximum. Since this amplitude is constrained by  $\mu$  distortion, it imposes a lower bound on this ratio. Such a bound leads to an inadequate duration of USR, producing a sharp dip, instead of a null in the power spectrum.

The second model we shall consider is an inflationary scenario driven by the Higgs field that is coupled non-minimally to gravitation [14, 41–43]. The model is known

as critical-Higgs inflation (CH), and the effective potential in this scenario contains a point of inflection, which leads to an epoch of USR thereby enhancing the scalar power over small scales. The potential describing the model can be written as

$$V(\phi) = V_0 \frac{[1 + a (\ln z)^2] z^4}{[1 + c (1 + b \ln z) z^2]^2}, \quad (5)$$

where  $z = \phi/\phi_0$ . As in the case of ST, we choose the parameters of the potential so that the power spectrum is consistent with COBE normalization on large scales and with the constraints from spectral distortions on smaller scales. For the values of the parameters we work with (in this regard, see the supplementary material), we find that a dip in the power spectrum occurs at around  $k_{\text{dip}} = 7.6 \text{ Mpc}^{-1}$  and the power reaches its maximum amplitude at around  $5.5 \times 10^9 \text{ Mpc}^{-1}$ . The  $\mu$  distortion arising due to this spectrum is found to be about  $2.0 \times 10^{-5}$ , which is within the FIRAS bound [12, 39].

It is known that, in single field models of inflation, if the enhancement in power is to be achieved over wavenumbers that are close to the CMB scales, there can arise a tension between the value of the scalar spectral index  $n_s$  in the model and the constraint on the parameter from the CMB data (for recent discussions, see Refs. [44, 45]). In the ST and CH models, the value of  $n_s$  at the pivot scale of  $k_* = 0.05 \text{ Mpc}^{-1}$  turns out to be 0.9995 and 0.78, respectively, which are well away from the mean value of 0.96 from Planck [46]. One way to circumvent this challenge is to construct inflationary potentials using the desired behavior of  $\epsilon_1(N)$  and, interestingly, it can be shown that these reconstructed potentials too contain a point of inflection [10]. In other words, using methods of reconstruction, it is possible to arrive at potentials numerically that are consistent with the CMB data on large scales and lead to a dip in the power spectrum over  $1 \lesssim k \lesssim 10 \text{ Mpc}^{-1}$  (for details, see the supplementary material).

We find that the features around the dip have the same characteristics in the reconstructed scenario as in the ST and CH models. Therefore, we shall proceed by considering these models and examining their imprints on the 21 cm signal. We evolve the background and compute the scalar power and bi-spectra numerically (see the supplementary material for details, which includes Refs. [47–51]). In Figs. 1 and 4 (see App. I), we have presented the inflationary scalar power and bi-spectra, i.e.  $\mathcal{P}_s(k)$  and  $\mathcal{B}_s(\mathbf{k}_1, \mathbf{k}_2, \mathbf{k}_3)$ , that arise in the ST and CH models, for the values of the parameters we have worked with.

We note two related points regarding the bispectra. Firstly, in contrast to the power spectrum which is a positive definite quantity, the bispectra can cross zero when departures from slow roll arise. Hence, it may vanish at locations other than  $k_{\text{dip}}$ . However, these nulls are dependent on the nature of the integrals involved in the computation of the bispectrum and may not be observed

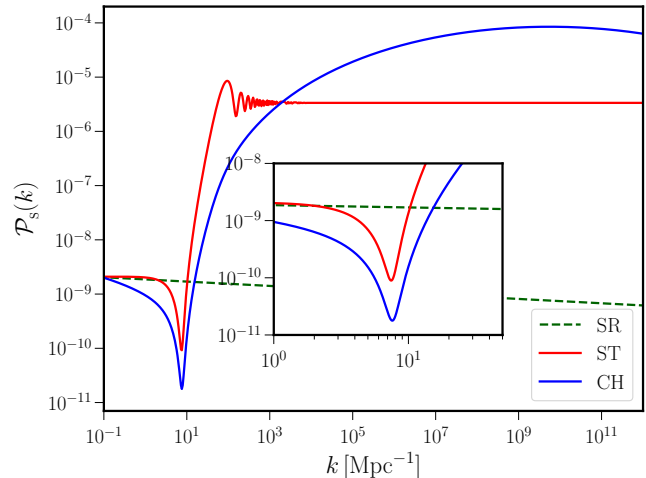


FIG. 1. The inflationary scalar power spectra arising in ST and CH models are illustrated for parameters that are consistent with the constraints on spectral distortions from FIRAS. We have also plotted the nearly scale invariant spectrum that may be obtained from a typical SR model of inflation. The inset highlights the dip in the spectra at  $k = 7.6 \text{ Mpc}^{-1}$ , and we work with parameters such that the dip occurs over wavenumbers where the HI signal is expected to be most sensitive to the primordial power spectrum.

at the same locations in the higher order correlations. Therefore, they are not as generic as the dip of interest, which will be located at  $k_{\text{dip}}$  in the higher order correlations as well. Hence, in models wherein a deviation from slow roll arises due to an epoch of USR, the bispectra are *guaranteed* to exhibit a sharp dip at  $k_{\text{dip}}$ . Secondly, note that the power and bispectra in the Starobinsky model rise more sharply than in the Higgs model. This can be attributed to the sharp change in the slope of the potential in the former model [34, 52]. Moreover, for the models of interest, the dip in the power spectrum occurs at the linear order of the perturbations. Though there may arise corrections to the power spectrum due to higher order correlations, we have checked, for instance, that the corrections due to the bispectrum are negligible for the parameters considered.

*Imprints on pre-ionization HI signal:* We now turn to discuss the imprints of the inflationary power and bi-spectra with sharp dips that we have obtained on the 21 cm signal of HI from the Dark Ages. We briefly outline the essential points. In the rest frame of a hydrogen atom, the hyperfine splitting of the ground state causes an energy difference that corresponds to the wavelength of  $\lambda = 21.1 \text{ cm}$ . The spin temperature  $T_s$  of this line is determined by three processes taking place in the early universe: emission and absorption of CMB photons with a black body temperature  $T_{\text{CMB}}$ , collisions with atoms, and the mixing of the two levels caused by Ly- $\alpha$  photons (i.e. the Wouthuysen-Field effect). The spin temperature  $T_s$  can be expressed in terms of  $T_{\text{CMB}}$ , the gas kinetic temperature  $T_K$ , and

the color temperature of the Lyman- $\alpha$  photons  $T_\alpha$ , as follows [25, 53]:  $T_s = (T_{\text{CMB}} + y_c T_K + y_\alpha T_\alpha)/(1 + y_c + y_\alpha)$ . In this expression,  $y_c$  and  $y_\alpha$  determine the efficacy of the collisions between the hydrogen atoms and of the hydrogen atoms with the Lyman- $\alpha$  photons, respectively. Note that,  $y_c \propto n_{\text{HI}}$  and  $y_\alpha \propto n_\alpha$ , where  $n_{\text{HI}}$  and  $n_\alpha$  denote the number density of HI and the Lyman-alpha photons. HI emits or absorbs 21 cm radiation from the CMB depending on whether  $T_s$  is greater than or less than  $T_{\text{CMB}}$ . This global temperature difference is observable and can be expressed as [25, 54, 55]

$$\Delta T_b(z) \simeq 30 \left(1 - \frac{T_{\text{CMB}}}{T_s}\right) \left(\frac{1+z}{10}\right)^{1/2} \left(\frac{\Omega_b h^2}{0.022}\right) \text{mK}. \quad (6)$$

The signal is observable at the frequency of 1420 MHz/(1+z) at a given redshift  $z$ .

Before the onset of the era of cosmic dawn,  $y_\alpha = 0$  and the dynamics of  $T_s$  is entirely determined by the other two processes. For  $z \gtrsim 50$ , collisions dominate and hence  $T_s \simeq T_K$ . As  $T_K \simeq T_{\text{CMB}}$  for  $z \gtrsim 200$ ,  $T_s$  relaxes to  $T_{\text{CMB}}$  in this redshift range and the observable signal is negligible. At lower redshifts ( $z \lesssim 150$ ),  $T_K$  falls adiabatically as  $1/a^2$  and, as  $T_s \simeq T_K$ , HI is observable in absorption. At even smaller redshifts, owing to the dilution of the gas, the collisional coupling becomes progressively weaker and  $T_s$  relaxes to  $T_{\text{CMB}}$ , causing the HI signal to diminish.

We have relegated the details of the computation of the power and bi-spectra of the HI signal to App. II. In Fig. 2, we present the HI intensity power spectrum arising in the ST and CH models at the redshifts of  $z = 27$  and  $z = 50$ . In the figure, we have also included the results from a typical SR model, along with the contribution from PF. In Fig. 3, we have illustrated the HI intensity bispectrum arising in the ST and CH models at two redshifts in the equilateral, squeezed and flattened limits, along with the contribution from PF.

Our main findings, shown in Figs. 2 and 3, clearly indicate that, in the presence of an epoch of USR, there arises a significant dip in the HI intensity power and bispectra over the scales  $1 \lesssim k \lesssim 10 \text{Mpc}^{-1}$ , when compared to a typical SR scenario. The HI signal arising from the inflationary bispectrum is seen to be smaller than the contribution from PF by many orders of magnitude. As the Poisson contribution to the bispectrum depends on the HI power spectrum [cf. Eq. (10)], the detection of this signal would provide further evidence of the presence of a null or a dip in the inflationary power spectrum.

*Sensitivity:* We now explore the feasibility of the detection of the HI intensity power spectrum over scales of interest. As can be seen in Fig. 2, our main predictions are over the scales  $1 \lesssim k \lesssim 100 \text{Mpc}^{-1}$ . The signal strength at such scales is of the order of 10–1000 (mK)<sup>2</sup> in the frequency range 25–50 MHz, for the redshift range  $z \simeq 25$ –50. While the signal at  $z \simeq 25$  is accessible to SKA-Low (see, e.g., Ref. [56]), we expect the signal at  $z \simeq 50$  to be more pristine (i.e. less contaminated by astrophysical processes close to the era of cosmic dawn) and dominant. Such a signal could be explored by planned lunar missions [27–29]. Under suitable assumptions (for a detailed discussion

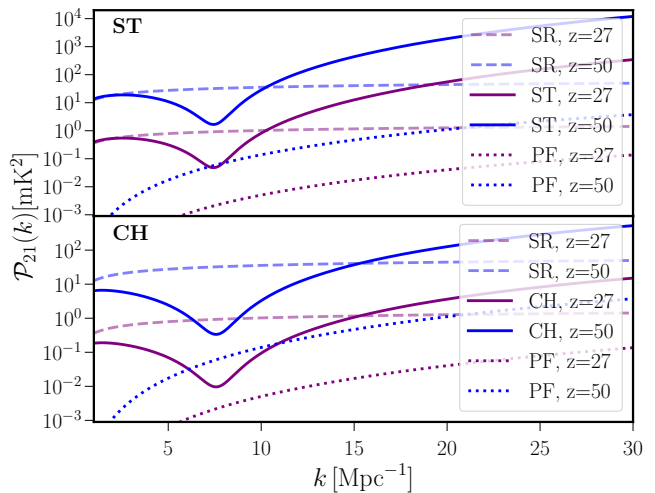


FIG. 2. The HI intensity power spectra arising from the ST and CH models have been plotted at the redshifts of  $z = 27$  and  $z = 50$ . For comparison, we have also presented the HI intensity power spectra arising in a SR scenario leading to a nearly scale invariant, power law primordial scalar power spectrum. We have also included the power spectra due to PF at the corresponding redshifts.

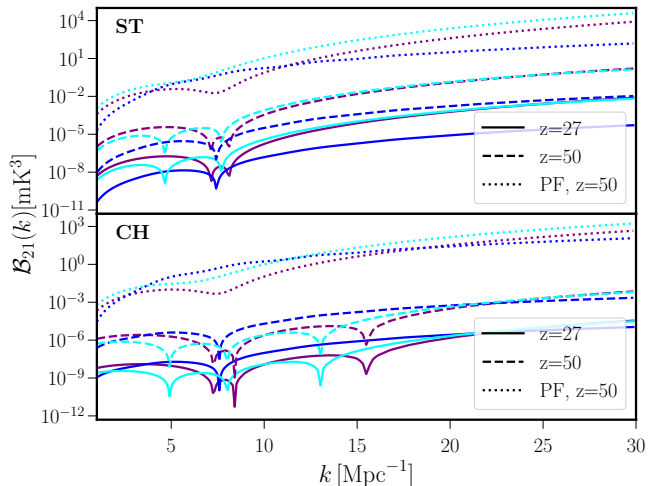


FIG. 3. The HI intensity bispectra arising from the ST and CH models have been presented in the equilateral, squeezed and the flattened limits with the same choice of colors as in Fig. 4. We have focused around  $k_{\text{dip}}$  and we have set  $k_{\text{sq}} = k/100$  to arrive at the behavior in the squeezed limit. The associated PF have also been indicated.

and methodology, see the supplementary material, which includes Refs. [57–59]), the brightness temperature sensitivity of 1–10 (mK)<sup>2</sup> can be achieved for the scales of interest. A comparison with Fig. 2 immediately suggests that the attainable sensitivity should allow the detection of the dip due to the epoch of USR in the HI power spectrum.

*Conclusions:* In models of inflation driven by a single, canonical scalar field, an extended phase of USR leads

to a *null* in *all* the primordial correlations at a specific wavenumber  $k_{\text{dip}}$ . We have considered scenarios in which the null in the primordial correlations occurs over wavenumbers  $1 \lesssim k_{\text{dip}} \lesssim 10 \text{ Mpc}^{-1}$ . We show that future experiments should have the sensitivity to detect a damping of power in the HI signal due to the nulls at the level of the power and bi-spectra.

*Acknowledgements:* SB thanks Yi-Peng Wu for helpful discussions. HVR acknowledges support from the Indian Institute of Science Education and Research Kolkata through postdoctoral fellowship. LS acknowledges support from the Science and Engineering Research Board, Department of Science and Technology, Government of India, through the Core Research Grant CRG/2018/002200. SB is supported by funding from the European Union's Horizon 2020 research and innovation programme under grant agreement No. 101002846 (ERC CoG ‘‘CosmoChart’’) as well as support from the Initiative Physique des Infinis (IPI), a research training program of the Ixex SUPER at Sorbonne Universit e.

### Appendix I: Inflationary scalar bispectrum

In this appendix, we have plotted the bispectra in the equilateral (i.e. when  $k_1 = k_2 = k_3$ ), squeezed (when  $k_1 \rightarrow 0$  and  $k_2 = -k_3 = k$ ) and flattened (when  $k_1 = k_2 = k$  and  $k_3 = 2k$ ) limits. In Fig. 4, we have illustrated the dimensionless quantities such as  $k^6 \mathcal{B}_s(k)$  in the equilateral and flattened limits, and  $k_1^3 k_3^3 \mathcal{B}_s(k)$  in the squeezed limit. We find that a dip in the bispectra arises in *all* the limits at the same location of the dip (viz. at  $k_{\text{dip}} = 7.6 \text{ Mpc}^{-1}$ ) in the power spectra.

### Appendix II: Computation of power and bi-spectra of 21 cm signal

In this appendix, we provide the details of the computation of power and bi-spectra of the HI intensity signal in terms of the primordial spectra.

At linear order in the perturbations, the density fluctuations in HI follow the baryonic perturbations. This allows us to express the fluctuating component of the HI signal in the pre-reionization epoch as  $\delta T(\mathbf{x}) = \Delta T_b(z) \delta_{\text{HI}}(\mathbf{x})$ , where  $\delta_{\text{HI}}(\mathbf{x})$  denotes the inhomogeneities in the density of the neutral gas. We shall ignore the redshift-space distortions in our discussion. At small scales, these perturbations are wiped out due to acoustic damping in the pre-recombination era and are re-generated by dark matter potential wells in the post-recombination era. In linear theory, the baryonic perturbations can be expressed in terms of the inflationary scalar power spectrum as  $\mathcal{P}_{\text{HI}}(k, z) = T^2(k, z) \mathcal{P}_s(k)$ , where  $T(k, z)$  is the transfer function for baryons defined such that  $T(k, z)$  tends to unity for small  $k$  (see, for instance, Ref. [60]). This allows

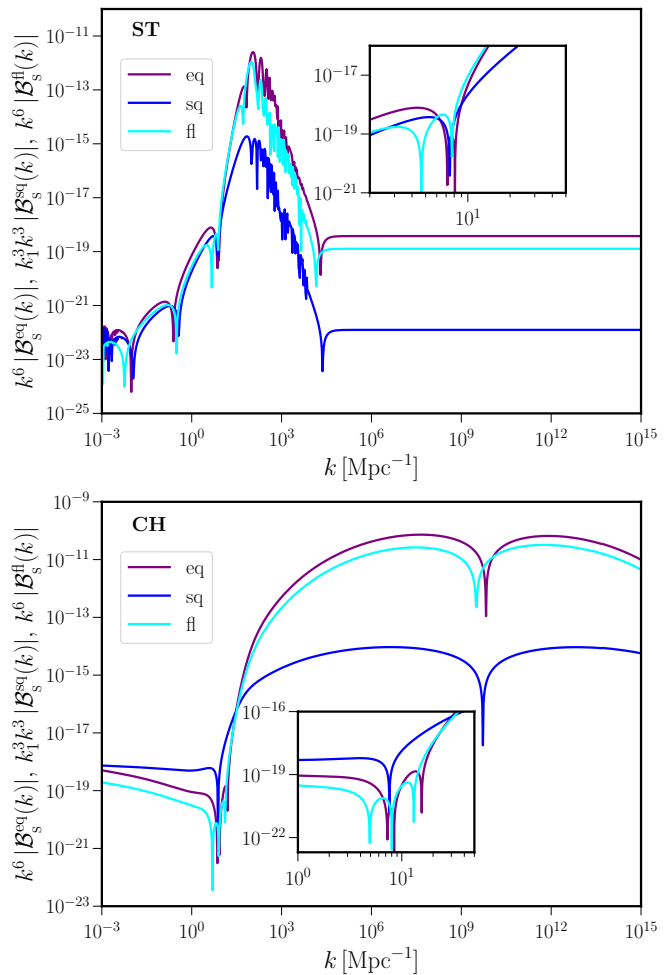


FIG. 4. The scalar bispectra arising in the ST and CH models have been illustrated in the equilateral (eq), squeezed (sq) and flattened (fl) limits. As highlighted in the insets, the bispectra also exhibit a sharp dip at the same location (i.e. at  $7.6 \text{ Mpc}^{-1}$ ) as the power spectra in the previous figure.

us to write the HI intensity power spectrum at a redshift  $z$  in  $(\text{mK})^2$  as follows:

$$\mathcal{P}_{21}(k, z) = [\Delta T_b(z)]^2 T^2(k, z) \mathcal{P}_s(k). \quad (7)$$

At any redshift, a fraction of baryons, say,  $f_c$ , collapse to form halos. The baryons in these halos remain neutral, since for the parameters of interest, the masses of collapsed halos are  $\mathcal{O}(10^6 M_\odot)$  and the virial temperature of these halos is less than 1000 K, too small to ionize the gas via collisional processes (we evade the free-free constraints on the excess matter power discussed in Ref. [61]; also see Ref. [62]). The HI intensity power spectrum from PF at a given redshift in  $(\text{mK})^2$  is given by (in this context, see, for instance, Ref. [63])

$$\mathcal{P}_{21}^{\text{PF}}(k, z) = [f_c \Delta T_b(z)]^2 \frac{k^3}{2\pi^2} \frac{1}{\bar{n}}, \quad (8)$$

where  $\bar{n}$  is the mean comoving number density of halos. The collapsed fraction  $f_c$  and the number density of halos  $\bar{n}$  at any redshift can be computed using the Press-Schechter formalism. For instance, in the CH model, at  $z = 50$ ,  $f_c = 0.17$  and  $\bar{n} = 18754 \text{ Mpc}^{-3}$ , while at  $z = 100$ ,  $f_c = 7 \times 10^{-3}$  and  $\bar{n} = 1549 \text{ Mpc}^{-3}$ . At both redshifts, the mass function is dominated by halos of mass  $M \lesssim 5 \times 10^5 M_\odot$ . At  $z = 27$ ,  $\bar{n} = 27638 \text{ Mpc}^{-3}$  and  $f_c = 0.45$ , with halos of  $M \lesssim 2 \times 10^6 M_\odot$  making the most significant contribution to the mass function. We have plotted the spectra  $\mathcal{P}_{21}(k, z)$  and  $\mathcal{P}_{21}^{\text{PF}}(k, z)$  for the ST and CH models in Fig. 2.

Given the scalar bispectrum  $\mathcal{B}_s(\mathbf{k}_1, \mathbf{k}_2, \mathbf{k}_3)$  generated during inflation, the HI intensity bispectrum at any redshift can be expressed in units of  $(\text{mK})^3$  as

$$\mathcal{B}_{21}(\mathbf{k}_1, \mathbf{k}_2, \mathbf{k}_3, z) = \frac{[\Delta T_b(z)]^3}{2\pi^2} T(k_1, z) T(k_2, z) T(k_3, z) \times \frac{k_1^3 k_2^3 k_3^3}{(k_1^3 + k_2^3 + k_3^3)} \mathcal{B}_s(\mathbf{k}_1, \mathbf{k}_2, \mathbf{k}_3). \quad (9)$$

Also, the bispectrum from PF of discrete sources is given by (see e.g., Ref. [63])

$$\mathcal{B}_{21}^{\text{PF}}(\mathbf{k}_1, \mathbf{k}_2, \mathbf{k}_3, z) = \frac{f_c^3 k_1^3 k_2^3 k_3^3 \Delta T_b(z)}{(k_1^3 + k_2^3 + k_3^3) \bar{n}} \left\{ -\frac{2[\Delta T_b(z)]^2}{\bar{n}} + \frac{\mathcal{P}_{21}(k_1)}{k_1^3} + \frac{\mathcal{P}_{21}(k_2)}{k_2^3} + \frac{\mathcal{P}_{21}(k_3)}{k_3^3} \right\}. \quad (10)$$

We have presented the HI intensity bispectrum at redshifts of  $z = 27$  and  $50$  in Fig. 3 along with the corresponding PF computed at  $z = 50$ .

**Supplemental material for  
'Observing nulling of primordial correlations via the  
21 cm signal'**

In the following sections, we shall gather material that supplement the discussions in the manuscript.

**Starobinsky functions**

The scalar power spectrum in the ST model can be analytically calculated to be [32, 34, 35]

$$\mathcal{P}_s(k) = \mathcal{P}_s^0 \left( \frac{A_+}{A_-} \right)^2 \left[ I(k) + I_c(k) \cos\left(\frac{2k}{k_0}\right) + I_s(k) \sin\left(\frac{2k}{k_0}\right) \right], \quad (11)$$

where  $k_0$  is the wavenumber that leaves the Hubble radius when  $\phi = \phi_0$ , while the quantities  $\mathcal{P}_s^0$  and  $\epsilon_{1-}$  are related to the parameters of the potential by the relations

$$\mathcal{P}_s^0 \simeq \frac{V_0}{24 \pi^2 M_{\text{Pl}}^4 \epsilon_{1+}}, \quad \epsilon_{1+} \simeq \frac{M_{\text{Pl}}^2}{2} \left( \frac{A_+}{V_0} \right)^2. \quad (12)$$

The functions  $I(k)$ ,  $I_c(k)$  and  $I_s(k)$  that appear in the power spectrum above are given by

$$I(k) = 1 + \frac{9}{2} \left( \frac{\Delta A}{A_+} \right)^2 \left( \frac{k_0}{k} \right)^2 \times \left[ 1 + 2 \left( \frac{k_0}{k} \right)^2 + \left( \frac{k_0}{k} \right)^4 \right], \quad (13a)$$

$$I_c(k) = \frac{3}{2} \frac{\Delta A}{A_+} \left( \frac{k_0}{k} \right)^2 \left[ 3 \frac{\Delta A}{A_+} - 4 - 3 \frac{\Delta A}{A_+} \left( \frac{k_0}{k} \right)^4 \right], \quad (13b)$$

$$I_s(k) = -3 \frac{\Delta A}{A_+} \frac{k_0}{k} \times \left[ 1 + \left( \frac{3 \Delta A}{A_+} - 1 \right) \left( \frac{k_0}{k} \right)^2 + 3 \frac{\Delta A}{A_+} \left( \frac{k_0}{k} \right)^4 \right], \quad (13c)$$

where  $\Delta A = A_- - A_+$ . Actually, we need to smoothen the potential to be able to compute the spectrum numerically (in this context, see Refs. [34, 35, 38]; also see the discussion that follows). We find that the above analytical form for the power spectrum matches the numerical result very well.

**Parameters and background evolution**

In the case of the ST model, for numerical analysis, we smoothen the potential [cf. Eq. (4) of the manuscript] and

work with the potential given by [37, 38]

$$V(\phi) = V_0 + \frac{1}{2} (A_+ + A_-) (\phi - \phi_0) + \frac{1}{2} (A_+ - A_-) (\phi - \phi_0) \tanh\left(\frac{\phi - \phi_0}{\Delta\phi}\right). \quad (14)$$

We set  $V_0 = 2.48 \times 10^{-11} M_{\text{Pl}}^4$  and  $A_+ = V_0/(100 M_{\text{Pl}})$  to achieve COBE normalization over the CMB scales. We choose  $A_- = V_0/(4 \times 10^3 M_{\text{Pl}})$  and  $\phi_0 = 0.5628 M_{\text{Pl}}$ . If we choose the initial value of the field and the first SR parameter to be  $\phi_i = 0.84348 M_{\text{Pl}}$  and  $\epsilon_{1i} = 4.0 \times 10^{-5}$ , respectively, we find that the pivot scale leaves the Hubble radius around 6.4 e-folds before field crosses  $\phi_0$ . These choices for the parameters leads to a rise in power on smaller scales that is consistent with the FIRAS constraints on  $\mu$ -distortions [12].

In the CH model, we choose the values of the parameters to be  $V_0 = 7.05 \times 10^{-8} M_{\text{Pl}}^4$  and  $\phi_0 = 1 M_{\text{Pl}}$ . The dimensionless parameters  $a$  and  $b$  are related to  $c$  and the location of the point of inflection, say,  $z_c$ . Choosing the parameters  $(c, z_c) = (2.850, 0.820)$  leads to  $(a, b) = (1.694, 0.601)$ . The value of the parameter  $b$  is then fine tuned to achieve the desired duration of the USR epoch so that the rise in power is consistent with the constraints from FIRAS [12]. For these values of the model parameters and with the initial value of field  $\phi_i = 5.55 M_{\text{Pl}}$  and the first SR parameter  $\epsilon_{1i} = 10^{-3}$ , we achieve about 70 e-folds of inflation. We set the pivot scale to exit the Hubble radius at 46.5 e-folds before the end of inflation. The epoch of USR begins as the field crosses the point  $\phi = 0.82 M_{\text{Pl}}$ , around 40 e-folds before the end of inflation.

**Reconstructing a model with a phase of USR**

We had pointed out that, at the pivot scale of  $0.05 \text{ Mpc}^{-1}$ , the ST and CH models lead to a scalar spectral index that is quite removed from the mean value of  $n_s = 0.96$  suggested by Planck [46]. We had also mentioned that, it is challenging to arrive at a model involving a single, canonical scalar field that leads to a significant enhancement of power on small scales and is consistent with the constraints from Planck on the CMB scales [44, 45]. To overcome this issue, one may resort to the reconstruction of a scenario of inflation using a parametric modeling of the first SR parameter  $\epsilon_1$ . We find that the following functional form of  $\epsilon_1(N)$  leads to the desired behavior of the background and power spectra (for a detailed discussion, see Ref. [10]):

$$\epsilon_1(N) = \epsilon_{1a} (1 + \epsilon_{2a} N) \left[ 1 - \tanh\left(\frac{N - N_1}{\Delta N_1}\right) \right] + \epsilon_{1b} + \exp\left(\frac{N - N_2}{\Delta N_2}\right), \quad (15)$$



where the quantities  $(\epsilon_{1a}, \epsilon_{2a}, \epsilon_{1b}, N_1, N_2, \Delta N_1, \Delta N_2)$  are parameters which we shall choose suitably. The parameters  $(\epsilon_{1a}, \epsilon_{2a})$  help to achieve appropriate values for the scalar spectral index and the tensor-to-scalar ratio over the CMB scales. While the parameters  $(N_1, \Delta N_1, \epsilon_{1a}, \epsilon_{1b})$  control the onset and duration of the epoch of USR, the parameters  $(N_2, \Delta N_2)$  regulate the behavior of the background after the USR phase until the termination of inflation. We have chosen the values of these parameters such that the dip in the power spectrum arises at the desired location and inflation is terminated after 60 e-folds. The values of the parameters we have worked with are as follows:  $(\epsilon_{1a}, \epsilon_{2a}, N_1, \Delta N_1, \epsilon_{1b}, N_2, \Delta N_2) = (10^{-4}, 0.05, 16.5, 0.3, 5 \times 10^{-7}, 60, 1)$ . In Fig. 5, we have illustrated the potential arrived at numerically from the above form of the first SR parameter (i.e. the reconstructed scenario, RS) as well as the resulting scalar power spectrum. Note that the resulting scalar power spectrum from the RS closely resembles the spectrum in the ST model around  $k_{\text{dip}}$ .

### Computation of scalar power and bi-spectrum

Let  $\mathcal{R}_{\mathbf{k}}$  denote the Fourier modes associated with the curvature perturbation  $\mathcal{R}$ . Recall that the scalar power spectrum  $\mathcal{P}_s(k)$  is defined through the relation

$$\langle \hat{\mathcal{R}}_{\mathbf{k}}(\eta_e) \hat{\mathcal{R}}_{\mathbf{k}'}(\eta_e) \rangle = \frac{(2\pi)^2}{2k^3} \mathcal{P}_s(k) \delta^{(3)}(\mathbf{k} + \mathbf{k}'), \quad (16)$$

where  $\eta_e$  denotes the conformal time close to the end of inflation and the expectation value on the left hand side is to be taken in the Bunch-Davies vacuum. In terms of the positive frequency Fourier modes that describe the curvature perturbations, say,  $f_k$ , the power spectrum is given by

$$\mathcal{P}_s(k) = \frac{k^3}{2\pi^2} |f_k|^2. \quad (17)$$

The primordial scalar bispectrum in Fourier space, denoted as  $\mathcal{B}_s(\mathbf{k}_1, \mathbf{k}_2, \mathbf{k}_3)$ , is defined through the relation

$$\langle \hat{\mathcal{R}}_{\mathbf{k}_1}(\eta_e) \hat{\mathcal{R}}_{\mathbf{k}_2}(\eta_e) \hat{\mathcal{R}}_{\mathbf{k}_3}(\eta_e) \rangle = (2\pi)^3 \mathcal{B}_s(\mathbf{k}_1, \mathbf{k}_2, \mathbf{k}_3) \times \delta^{(3)}(\mathbf{k}_1 + \mathbf{k}_2 + \mathbf{k}_3), \quad (18)$$

with the expectation value on the left hand side to be evaluated in the perturbative vacuum [47–49]. The bispectrum  $\mathcal{B}_s(\mathbf{k}_1, \mathbf{k}_2, \mathbf{k}_3)$  can be calculated using the third order action governing the perturbations and the standard rules of perturbative quantum field theory [34, 50]. It can be shown that, in the situations of our interest, the scalar bispectrum can be expressed as (see, for instance,

Refs. [10, 34, 51])

$$\mathcal{B}_s(\mathbf{k}_1, \mathbf{k}_2, \mathbf{k}_3) = \frac{M_{\text{Pl}}^2}{(2\pi)^{9/2}} \sum_{C=1}^6 \left[ f_{k_1}(\eta_e) f_{k_2}(\eta_e) f_{k_3}(\eta_e) \times B_C(\mathbf{k}_1, \mathbf{k}_2, \mathbf{k}_3) + \text{complex conjugate} \right] + \frac{1}{(2\pi)^{9/2}} \mathcal{B}_7(\mathbf{k}_1, \mathbf{k}_2, \mathbf{k}_3), \quad (19)$$

where  $f_k$  are the positive frequency Fourier modes associated with the curvature perturbation we mentioned above. The quantities  $B_C(\mathbf{k}_1, \mathbf{k}_2, \mathbf{k}_3)$  represent six integrals that involve the scale factor, the slow roll parameters, the mode functions  $f_k$  and their time derivatives  $f'_k$ . They correspond to the six bulk terms appearing in the cubic order action and are described by the following expressions

$$B_1(\mathbf{k}_1, \mathbf{k}_2, \mathbf{k}_3) = 2i \int_{\eta_i}^{\eta_e} d\eta a^2 \epsilon_1^2 \left( f_{k_1}^* f_{k_2}^* f_{k_3}^* + \text{two permutations} \right), \quad (20a)$$

$$B_2(\mathbf{k}_1, \mathbf{k}_2, \mathbf{k}_3) = -2i (\mathbf{k}_1 \cdot \mathbf{k}_2 + \text{two permutations}) \times \int_{\eta_i}^{\eta_e} d\eta a^2 \epsilon_1^2 f_{k_1}^* f_{k_2}^* f_{k_3}^*, \quad (20b)$$

$$B_3(\mathbf{k}_1, \mathbf{k}_2, \mathbf{k}_3) = -2i \int_{\eta_i}^{\eta_e} d\eta a^2 \epsilon_1^2 \left( \frac{\mathbf{k}_1 \cdot \mathbf{k}_2}{k_2^2} f_{k_1}^* f_{k_2}^* f_{k_3}^* + \text{five permutations} \right), \quad (20c)$$

$$B_4(\mathbf{k}_1, \mathbf{k}_2, \mathbf{k}_3) = i \int_{\eta_i}^{\eta_e} d\eta a^2 \epsilon_1 \epsilon_2' \left( f_{k_1}^* f_{k_2}^* f_{k_3}^* + \text{two permutations} \right), \quad (20d)$$

$$B_5(\mathbf{k}_1, \mathbf{k}_2, \mathbf{k}_3) = \frac{i}{2} \int_{\eta_i}^{\eta_e} d\eta a^2 \epsilon_1^3 \left( \frac{\mathbf{k}_1 \cdot \mathbf{k}_2}{k_2^2} f_{k_1}^* f_{k_2}^* f_{k_3}^* + \text{five permutations} \right), \quad (20e)$$

$$B_6(\mathbf{k}_1, \mathbf{k}_2, \mathbf{k}_3) = \frac{i}{2} \int_{\eta_i}^{\eta_e} d\eta a^2 \epsilon_1^3 \left[ \frac{k_1^2 (\mathbf{k}_2 \cdot \mathbf{k}_3)}{k_2^2 k_3^2} f_{k_1}^* f_{k_2}^* f_{k_3}^* + \text{two permutations} \right]. \quad (20f)$$

The term  $\mathcal{B}_7(\mathbf{k}_1, \mathbf{k}_2, \mathbf{k}_3)$  corresponds to a temporal boundary term in the cubic order action and is given by

$$\mathcal{B}_7(\mathbf{k}_1, \mathbf{k}_2, \mathbf{k}_3) = -i M_{\text{Pl}}^2 [f_{k_1}(\eta_e) f_{k_2}(\eta_e) f_{k_3}(\eta_e)] \times \left[ a^2 \epsilon_1 \epsilon_2 f_{k_1}^*(\eta) f_{k_2}^*(\eta) f_{k_3}^*(\eta) + \text{two permutations} \right]_{\eta_i}^{\eta_e} + \text{complex conjugate}. \quad (21)$$



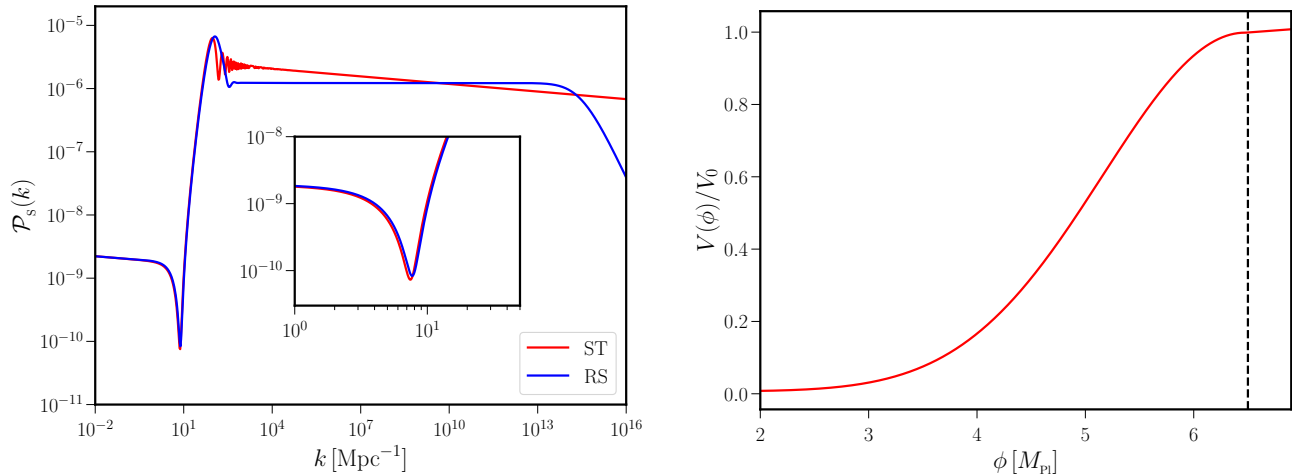


FIG. 5. The scalar power spectrum  $\mathcal{P}_s(k)$  arising from the RS involving an epoch of USR has been presented along with the power spectrum from the ST model (on the left). Notice that both the power spectra have identical shapes close to  $k_{\text{dip}}$  (as also highlighted in the inset). In the RS, the power spectrum decays at large wavenumbers due to the termination of inflation. We have also illustrated the form of the potential  $V(\phi)$  describing the RS (on the right). Interestingly, to the extent permitted by numerical analysis, we find that the reconstructed potential too contains a point of inflection around  $\phi = 6.5 M_{\text{pl}}$  (indicated by the black vertical line). The parameter  $V_0$  indicated has been taken to be  $3 H_1^2 M_{\text{pl}}^2$ , where  $H_1$  is the initial value of the Hubble parameter. We have chosen  $H_1 = 6.98 \times 10^{-6} M_{\text{pl}}$  so as to achieve COBE normalization of the scalar power spectrum over the CMB scales.

In SR scenarios, typically, one evolves the perturbations from well inside the Hubble radius (say, when  $k \simeq 10^2 a H$ ) to adequately late times when the modes are on super-Hubble scales (say, when  $k \simeq 10^{-5} a H$ ), to arrive at the power spectrum [51]. When there occur departures from SR, in particular, in the presence of an epoch of USR, it becomes important to evolve the perturbations until very late times, close to the end of inflation [10, 38]. These arguments broadly apply for the computation of the scalar bispectrum as well. However, note that, apart from numerically evaluating the mode functions, to obtain the bispectrum, we also need to carry out integrals over the mode functions, their time derivatives and the background quantities. Since the bispectrum, in general, involves three wavenumbers, we need to evolve the perturbations and carry out the integrals from the time when the smallest of the three wavenumbers of interest is well inside the Hubble radius to a time close to the end of inflation (for further details, see Ref. [10]). It is these procedures that we have adopted to arrive at the power and bi-spectra we have presented in this work.

### Sensitivity of an interferometric array to HI power spectrum

Let us assume that visibilities for a given baseline  $\mathbf{u}$ ,  $V_\nu(\mathbf{u})$ , corresponding to a statistically homogeneous process such as the HI signal or detector noise, are measured for  $n_\nu$  discrete frequency channels. The measured visibilities can be Fourier transformed from frequency space to

the delay space (see e.g. Ref. [24], and references therein) and correlated to obtain  $\langle V_\tau(\mathbf{u}) V_\tau(\mathbf{u}) \rangle$ , where  $\tau$  is the conjugate variable of the frequency difference between two maps. In discrete space,  $\tau = n/\Delta\nu$ , where  $n$  runs between zero and  $n_\nu/2$ , while  $\Delta\nu = \delta\nu n_\nu$  is the total bandwidth and  $\delta\nu$  is the channel width. The correlation in delay space can be related to the power spectrum as follows (for a detailed derivation see, for instance, Ref. [57], and references therein)

$$\langle V_\tau(\mathbf{u}) V_\tau(\mathbf{u}) \rangle \simeq \frac{\Delta\nu I_\nu^2 \Omega_p}{r_\nu^2 r'_\nu} P(k), \quad (22)$$

where  $r_\nu$  is the coordinate distance,  $r'_\nu \equiv dr_\nu/d\nu$ ,  $\Omega_p$  is the primary beam, and  $I_\nu = k T_B/\lambda_0^2$ . In delay space, different components of the wave vector  $k = \sqrt{k_\perp^2 + k_\parallel^2}$ , decomposed as modes on the plane of the sky  $\mathbf{k}_\perp$ , and along the line of sight  $k_\parallel$ , are related to the parameters of the radio interferometer as  $\mathbf{k}_\perp \simeq 2\pi \mathbf{u}_\nu/r_\nu$  and  $k_\parallel = 2\pi \tau/(dr_\nu/d\nu)$ .

Assuming the visibility correlation to be dominated by the detector noise and a baseline coverage that yields uniform noise<sup>1</sup>, one can obtain the error on the brightness

<sup>1</sup> In an integration time  $t_{\text{int}}$ , the total number of baselines is  $N(N-1)t_{\text{int}}/(2t_{\text{acc}})$ , where  $t_{\text{acc}}$  is the time for one measurement. For high density of baselines, the instantaneous baseline coverage is complete or it samples each UV pixel for a range of baselines (generally short baselines, e.g. MWA for baselines shorter than roughly  $200 \lambda_0$  [58]). Therefore, the total number of independent UV pixels remains  $N(N-1)/2$  after  $t = t_{\text{int}}$ . This yields uniform noise in each pixel in both UV and real space.

temperature fluctuations from the detector noise (for each primary beam and for non-redundant baselines):

$$\delta \left( \frac{T_B^2 k^3 P(k)}{2\pi^2} \right) \simeq \frac{T_{\text{sys}}^2 \Omega_p r'_\nu r_\nu^2 \delta\nu k^3}{2\pi^2 f^{1/2}(k) N \Delta\nu t_{\text{int}}}, \quad (23)$$

where  $T_{\text{sys}}$  is the system temperature,  $N$  is the number of antennas, and  $f(k)$  is the fraction of baseline in the range  $k$  and  $(k + dk)$ . Current (e.g. LOFAR) and future low-frequency radio interferometers have the capability to form and image in multi-beams. Multiple primary beams help to improve both the detector sensitivity and the sample variance. For  $n_p$  primary beams, the brightness temperature variance derived in Eq. (23) decreases by a factor of  $n_p^{1/2}$ .

It is our aim that the interferometer be sensitive to wavenumbers  $k \simeq 1\text{--}10 \text{ Mpc}^{-1}$ . We consider two cases: (a)  $k_\perp \gg k_\parallel$ , and (b)  $k_\parallel \gg k_\perp$ . When  $k_\perp \gg k_\parallel$ , the baseline is  $u \simeq k r_\nu / (2\pi)$ . For  $z \simeq 50$ , this gives a baseline length ( $b = u \lambda_0$ ) of nearly 200 km for  $k \simeq 10 \text{ Mpc}^{-1}$ . In three dimensions,  $f(k) \propto k^3$ , which causes the brightness temperature sensitivity to scale as  $k^{3/2}$  (see e.g. Ref. [59]). However, it is not easy to achieve uniform coverage in this case as the number of telescopes needed to achieve it scales as  $k^2$ . For instance, if uniform UV coverage could be achieved with 100 telescopes for  $k = 0.1 \text{ Mpc}^{-1}$  (e.g. MWA configuration, see Ref. [58]), then nearly  $10^4$  telescopes would be needed to reach the same goal for  $k = 1 \text{ Mpc}^{-1}$ . We therefore consider another novel method which is more suitable for the detection of the HI signal at small scales, viz. when  $k_\parallel \gg k_\perp$ . In this case,  $k \simeq k_\parallel$  and the baseline length does not play a role in determining the sensitivity of the array to a given Fourier mode. In this case,  $f_k = 1$  as all baselines contribute equally to the sensitivity for any scale for which  $k_\parallel \gg k_\perp$ .

We note that better sensitivity might be achieved in case (b) as  $f(k) = 1$ . However, the sensitivity scales as  $k^3$  for case (b) whereas it scales as  $k^{3/2}$  for case (a), so case (a) might be the method of choice at large scales. We choose the following parameters for computing the sensitivity at  $z = 50$  for case (b): integration time,  $t_{\text{int}} = 3 \times 10^7$ ; channel width,  $\delta\nu = 10 \text{ kHz}$ ; total bandwidth,  $\Delta\nu = 10 \text{ MHz}$ ; number of antennas,  $N = 5000$ ; system temperature,  $T_{\text{sys}} = 10^4 \text{ MHz}$ ; primary beam,  $\Omega_p = (4/57)^2$ ; number of beams,  $n_p = 100$ . This yields a brightness temperature variance  $\delta(T_B^2 k^3 P(k)/(2\pi^2)) \simeq (1 \text{ mK})^2$  at  $k = 3 \text{ Mpc}^{-1}$ . These parameters are within the reach of current technologies and might be realizable by SKA-II. However, ground-based telescopes might not work well at  $\nu = 30 \text{ MHz}$  needed to detect the signal due to ionospheric effects. Future space-based and lunar radio interferometers will evade this constraint [27–29]. We note that the sensitivity might be improved further with redundant baselines: if each baseline has redundancy  $M$ , the total number of independent baselines is nearly  $N^2/(2M)$ . While the non-redundant baselines yield incoherent addition, the

redundant baselines contribute coherently. This results in sensitivity on the noise power spectrum being better by a factor  $M^{-1}$ .

\* sbalaji@lpthe.jussieu.fr

† ragavendra.pdf@iiserkol.ac.in

‡ sethi@rri.res.in

§ silk@iap.fr

¶ sriram@physics.iitm.ac.in

- [1] J. Martin, C. Ringeval, and V. Vennin, *Phys. Dark Univ.* **5-6**, 75 (2014), arXiv:1303.3787 [astro-ph.CO].
- [2] J. Martin, C. Ringeval, R. Trotta, and V. Vennin, *JCAP* **03**, 039, arXiv:1312.3529 [astro-ph.CO].
- [3] M. A. Latif and A. Ferrara, *Publ. Astron. Soc. Austral.* **33**, e051 (2016), arXiv:1605.07391 [astro-ph.GA].
- [4] J. Garcia-Bellido and E. Ruiz Morales, *Phys. Dark Univ.* **18**, 47 (2017), arXiv:1702.03901 [astro-ph.CO].
- [5] G. Ballesteros and M. Taoso, *Phys. Rev. D* **97**, 023501 (2018), arXiv:1709.05565 [hep-ph].
- [6] C. Germani and T. Prokopec, *Phys. Dark Univ.* **18**, 6 (2017), arXiv:1706.04226 [astro-ph.CO].
- [7] K. Kannike, L. Marzola, M. Raidal, and H. Veermäe, *JCAP* **09**, 020, arXiv:1705.06225 [astro-ph.CO].
- [8] B. Carr and J. Silk, *Mon. Not. Roy. Astron. Soc.* **478**, 3756 (2018), arXiv:1801.00672 [astro-ph.CO].
- [9] I. Dalianis, A. Kehagias, and G. Tringas, *JCAP* **01**, 037, arXiv:1805.09483 [astro-ph.CO].
- [10] H. V. Ragavendra, P. Saha, L. Sriramkumar, and J. Silk, *Phys. Rev. D* **103**, 083510 (2021), arXiv:2008.12202 [astro-ph.CO].
- [11] H. V. Ragavendra, L. Sriramkumar, and J. Silk, *JCAP* **05**, 010, arXiv:2011.09938 [astro-ph.CO].
- [12] A. D. Gow, C. T. Byrnes, P. S. Cole, and S. Young, *JCAP* **02**, 002, arXiv:2008.03289 [astro-ph.CO].
- [13] J. Garcia-Bellido, M. Peloso, and C. Unal, *JCAP* **1612** (12), 031, arXiv:1610.03763 [astro-ph.CO].
- [14] H. V. Ragavendra, *Phys. Rev. D* **105**, 063533 (2022), arXiv:2108.04193 [astro-ph.CO].
- [15] S. Balaji, J. Silk, and Y.-P. Wu, *JCAP* **06** (06), 008, arXiv:2202.00700 [astro-ph.CO].
- [16] S. Balaji, G. Domenech, and J. Silk, (2022), arXiv:2205.01696 [astro-ph.CO].
- [17] N. C. Tsamis and R. P. Woodard, *Phys. Rev. D* **69**, 084005 (2004), arXiv:astro-ph/0307463.
- [18] W. H. Kinney, *Phys. Rev. D* **72**, 023515 (2005), arXiv:gr-qc/0503017.
- [19] C. T. Byrnes, P. S. Cole, and S. P. Patil, *JCAP* **06**, 028, arXiv:1811.11158 [astro-ph.CO].
- [20] G. Tasinato, (2020), arXiv:2012.02518 [hep-th].
- [21] P. S. Cole, A. D. Gow, C. T. Byrnes, and S. P. Patil, (2022), arXiv:2204.07573 [astro-ph.CO].
- [22] O. Özsoy and G. Tasinato, *Phys. Rev. D* **105**, 023524 (2022), arXiv:2111.02432 [astro-ph.CO].
- [23] G. Goswami and T. Souradeep, *Phys. Rev. D* **83**, 023526 (2011), arXiv:1011.4914 [astro-ph.CO].
- [24] M. F. Morales and J. S. B. Wyithe, *Ann.Rev.Astron.Astrophys* **48**, 127 (2010), arXiv:0910.3010.
- [25] J. R. Pritchard and A. Loeb, *Reports on Progress in Physics* **75**, 086901 (2012), arXiv:1109.6012.

- [26] J. B. Muñoz, E. D. Kovetz, A. Raccanelli, M. Kamionkowski, and J. Silk, *JCAP* **05**, 032, arXiv:1611.05883 [astro-ph.CO].
- [27] S. Furlanetto *et al.*, (2019), arXiv:1903.06212 [astro-ph.CO].
- [28] P. S. Cole and J. Silk, *Mon. Not. Roy. Astron. Soc.* **501**, 2627 (2021), arXiv:1912.02171 [astro-ph.CO].
- [29] L. V. E. Koopmans *et al.*, *Exper. Astron.* **51**, 1641 (2021), arXiv:1908.04296 [astro-ph.IM].
- [30] N. Afshordi, P. McDonald, and D. N. Spergel, *Astrophys. J. Lett.* **594**, L71 (2003), arXiv:astro-ph/0302035.
- [31] K. J. Mack and D. H. Wesley, (2008), arXiv:0805.1531 [astro-ph].
- [32] A. A. Starobinsky, *JETP Lett.* **55**, 489 (1992), [*Pisma Zh. Eksp. Teor. Fiz.*55,477(1992)].
- [33] F. Arroja and M. Sasaki, *JCAP* **1208**, 012, arXiv:1204.6489 [astro-ph.CO].
- [34] J. Martin and L. Sriramkumar, *JCAP* **01**, 008, arXiv:1109.5838 [astro-ph.CO].
- [35] V. Sreenath and L. Sriramkumar, *JCAP* **1410** (10), 021, arXiv:1406.1609 [astro-ph.CO].
- [36] H. V. Ragavendra, L. Sriramkumar, and J. Martin, manuscript in preparation (2022).
- [37] J. Martin, L. Sriramkumar, and D. K. Hazra, *JCAP* **1409** (09), 039, arXiv:1404.6093 [astro-ph.CO].
- [38] H. V. Ragavendra, D. Chowdhury, and L. Sriramkumar, (2020), arXiv:2003.01099 [astro-ph.CO].
- [39] J. Chluba *et al.*, (2019), arXiv:1909.01593 [astro-ph.CO].
- [40] M. McQuinn, *Annual Review of Astronomy and Astrophysics* **54**, 313 (2016).
- [41] J. M. Ezquiaga, J. Garcia-Bellido, and E. Ruiz Morales, *Phys. Lett.* **B776**, 345 (2018), arXiv:1705.04861 [astro-ph.CO].
- [42] F. Bezrukov, M. Pauly, and J. Rubio, *JCAP* **02**, 040, arXiv:1706.05007 [hep-ph].
- [43] M. Drees and Y. Xu, *Eur. Phys. J. C* **81**, 182 (2021), arXiv:1905.13581 [hep-ph].
- [44] L. Iacconi, H. Assadullahi, M. Fasiello, and D. Wands, (2021), arXiv:2112.05092 [astro-ph.CO].
- [45] A. Karam, N. Koivunen, E. Tomberg, V. Vaskonen, and H. Veermäe, (2022), arXiv:2205.13540 [astro-ph.CO].
- [46] N. Aghanim *et al.* (Planck), *Astron. Astrophys.* **641**, A6 (2020), arXiv:1807.06209 [astro-ph.CO].
- [47] J. M. Maldacena, *JHEP* **05**, 013, arXiv:astro-ph/0210603.
- [48] D. Seery and J. E. Lidsey, *JCAP* **06**, 003, arXiv:astro-ph/0503692.
- [49] X. Chen, *Adv. Astron.* **2010**, 638979 (2010), arXiv:1002.1416 [astro-ph.CO].
- [50] F. Arroja and T. Tanaka, *JCAP* **05**, 005, arXiv:1103.1102 [astro-ph.CO].
- [51] D. K. Hazra, L. Sriramkumar, and J. Martin, *JCAP* **05**, 026, arXiv:1201.0926 [astro-ph.CO].
- [52] A. A. Starobinsky, *Phys. Lett. B* **91**, 99 (1980).
- [53] G. B. Field, *Proceedings of the IRE* **46**, 240 (1958).
- [54] N. Y. Gnedin and P. A. Shaver, *Astrophys. J.* **608**, 611 (2004), astro-ph/0312005.
- [55] S. K. Sethi, *Mon. Not. Roy. Astron. Soc.* **363**, 818 (2005), astro-ph/0508172.
- [56] L. V. E. Koopmans *et al.*, *PoS AASKA14*, 001 (2015), arXiv:1505.07568 [astro-ph.CO].
- [57] S. Paul *et al.*, *Astrophys. J.* **833**, 213 (2016), arXiv:1610.07003 [astro-ph.CO].
- [58] R. B. Wayth, S. J. Tingay, C. M. Trott, D. Emrich, M. Johnston-Hollitt, B. McKinley, B. M. Gaensler, A. P. Beardsley, T. Boller, B. Crosse, *et al.*, *Publications of the Astronomical Society of Australia* **35** (2018).
- [59] S. R. Furlanetto, S. P. Oh, and E. Pierpaoli, *Phys. Rev. D* **74**, 103502 (2006), arXiv:astro-ph/0608385.
- [60] S. Dodelson, *Modern cosmology / Scott Dodelson. Amsterdam (Netherlands): Academic Press. ISBN 0-12-219141-2, 2003, XIII + 440 p.* (Academic Press, 2003).
- [61] K. T. Abe, T. Minoda, and H. Tashiro, *Phys. Rev. D* **105**, 063531 (2022), arXiv:2108.00621 [astro-ph.CO].
- [62] A. Cattaneo, I. Koutsouridou, E. Tollet, J. Devriendt, and Y. Dubois, *Mon. Not. Roy. Astron. Soc.* **497**, 279 (2020), arXiv:2005.05958 [astro-ph.GA].
- [63] P. J. E. Peebles, *The large-scale structure of the universe* (1980).